Geophysical methods reveal the soil architecture and subsurface stratigraphic heterogeneities across land-lake interfaces along Lake Erie

Solomon Ehosioke[1*], Moses B. Adebayo[1], Vanessa L. Bailey[2,1], Roberta Bittencourt Peixoto[1], Efemena D. Emmanuel[1], Fausto Machado-Silva[1], Peter J. Regier[3], Trisha Spanbauer[1], Shan Pushpajom Thomas[1], Nicholas D. Ward[3,4], Michael N. Weintraub[1,2], Kennedy O. Doro[1*]

[1]Department of Environmental Sciences, University of Toledo, OH, USA

[2]Biological Sciences Division, Pacific Northwest National Laboratory, Richland, WA, USA

[3]Coastal Sciences Division, Pacific Northwest National Laboratory, Sequim, WA, USA

[4]College of the Environment, University of Washington, Seattle, WA, USA

***Corresponding Author:** Solomon Ehosioke (solomon.ehosioke@utoledo.edu) and Kennedy O. Doro (kennedy.doro@utoledo.edu)

Key Points:

- Multiple geophysical methods were combined to investigate hydrostratigraphic heterogeneities across land-lake interfaces
- Apparent electrical conductivity maps matched soil maps from public database, with hydric soil units delineated as high conductivity zones
- Results from resistivity and radar methods are consistent with the surficial geology of the study area

Abstract

The land-lake interface is a unique zone where terrestrial and aquatic ecosystems meet, forming part of the Earth's most geochemically and biologically active zones. The unique characteristics of this interface are yet to be properly understood due to the inherently high spatiotemporal variability of subsurface properties, which are difficult to capture with the traditional soil sampling methods. Geophysical methods offer non-invasive techniques to capture variabilities in soil properties at a high resolution across various spatiotemporal scales. We combined electromagnetic induction (EMI), electrical resistivity tomography (ERT), and ground penetrating radar (GPR) with data from soil cores and in-situ sensors to investigate hydrostratigraphic heterogeneities across land-lake interfaces along the western basin of Lake Erie. Our Apparent electrical conductivity (ECa) maps matched soil maps from a public database with the hydric soil units delineated as high conductivity zones (ECa > 40 mS/m) and also detected additional soil units that were missed in the traditional soil maps. This implies that electromagnetic induction (EMI) could be relied upon for non-invasive characterization of soils in sampling-restricted sites where only non-invasive measurements are feasible. Results from ERT and GPR are consistent with the surficial geology of the study area and revealed variation in the vertical silty-clay and till sequence down to 3.5 m depth. These results indicate that multiple geophysical methods can be used to extrapolate soil properties and map stratigraphic structures at land-lake interfaces, thereby providing the missing information required to improve the earth system model (ESM) of coastal interfaces.

Plain Language Summary

The interface between land and lake is a very active zone where various geochemical and biological changes occur. The unique characteristics of this interface are not fully understood because subsurface properties vary in time and space, and thus difficult to measure with the traditional soil sampling methods. We used three geophysical methods and data from soil cores and in-situ sensors to investigate hydrological and stratigraphic heterogeneities across land-lake interfaces along the western basin of Lake Erie. Our electrical conductivity maps matched soil maps from a public database and also detected additional soil units that were missed in the traditional soil maps, and the high conductivity zones matched the hydric soil units. Additionally, our results from electrical resistivity and radar methods are consistent with the surficial geology of the study area and revealed variation in the vertical silty-clay and till sequence down to 3.5 m depth. This shows that electromagnetic induction could be used to characterize soils in sampling-restricted sites where only non-invasive measurements are feasible. We also show that multiple geophysical methods can be used to deduce soil properties and map stratigraphic structures at land-lake interfaces, this information is required to improve the earth system model of coastal interfaces.

1. Introduction

Soils are known to be very heterogeneous due to the variability in soil properties or soil taxonomic classes within an area (Maestre and Cortina, 2002; McBratney and Minasny, 2007), resulting from regional soil formation factors such as topography, parent material, climate, organisms and time (ODNR, 2018; Sposito 2023). At land-lake interfaces, or more generally terrestrial-aquatic interfaces (TAIs), heterogeneity in soil architecture is much more diverse. This is because the TAI is where terrestrial and aquatic ecosystems meet and interact, forming an active and dynamic zone where various hydrological and biogeochemical exchanges occur at various spatial and temporal scales, thereby introducing additional sources of heterogeneity in the TAI soils. The diverse heterogeneities embodied by coastal TAIs are usually not accounted for in current earth system models (ESMs) (Ward et al. 2020).

Soil architecture which refers to the close relationship between the arrangement of soil physical components in space and the functioning that such arrangement enables (Baveye et al. 2018; Vogel et al. 2022), is controlled by the spatial configuration of pore networks resulting from processes of root growth, wetting and drying dynamics, freeze-thawing cycles, tillage operations (Dexter 1988, Vogel et al. 2022). Other factors that control soil architecture include the metabolic activities of soil micro and macro fauna within a soil matrix, the cementing organic molecules and associated physicochemical exchanges (Dexter 1988, Vogel et al. 2022). Soil architecture thus serves as a complex heterogeneous biogeochemical interface that forms the basis for various soil functions such as water retention, root growth, nutrient cycling, carbon storage, functional biodiversity, solute transport, and contaminant degradation (Totsche et al. 2010; Vogel et al. 2022). The extent to which these factors will influence the soil architecture depends on the soil type as well as the characteristics of the ecosystem unit or study site. Although these key

processes that control soil architecture occur mostly at the pore scale, their effects extend to larger spatial scales (e.g., site to regional scales), as many hydrological and ecological soil functions are governed by the soil architecture (Stewart et al. 1990; Romero-Ruiz et al. 2019).

Soil architecture has been investigated either by the aggregate approach or the pore approach. The aggregate approach targets the stability and composition of isolated solid fragments, while the pore approach targets the pore structure as well as the pore-solid interfaces in undisturbed samples (Rabot et al. 2018; Vogel et al. 2022). The aggregate approach is challenged by the limited understanding of how matter and energy fluxes through the soil will be affected when isolated from the original soil matrix. It is expected that fluxes of liquid, gas, or nutrients will differ between an isolated soil volume compared to an undisturbed one (e.g. Kravchenko et al. 2019). The pore approach considers the importance of spatial position but just within the context of an undisturbed sample. Although the pore approach recognized that flow and mixing processes such as diffusion of dissolved organic carbon, bioturbation, and pore water dynamics create spatial heterogeneity in soil architecture, it does not account for such heterogeneity beyond limited core samples (e.g. Young et al. 2001).

Traditional methods of soil investigation, such as soil cores, hand augers, excavation, or sensors (e.g., Osborne and DeLaune, 2013) are point measurements that lack spatial resolution and may not adequately capture the spatial variabilities necessary to include in site to global scale models. Geophysical methods offer non-invasive techniques to capture spatial variability in soil properties at high resolution and across various spatiotemporal scales (e.g., Besson et al. 2013; Krueger et al. 2013; Emmanuel et al. 2023). Romero-Ruiz et al. (2018) reviewed the potential of harnessing geophysical techniques for the characterization of soil architecture and identified geoelectrical and electromagnetic methods among a spectrum of geophysical methods as ideal for soil

architecture characterization. Due to their sensitivity to soil hydrological states, these methods, such as electromagnetic imaging (EMI) (e.g. Corwin and Lesch, 2005; Brechet et al. 2012; Doolittle and Brevik, 2014; Emmanuel et al. 2023), electrical resistivity tomography (ERT) (e.g. Michot et al. 2003; Kizhlo and Kanbergs, 2009; Besson et al. 2004, 2013; Doro et al. 2013), induced polarization (IP) (e.g. Kemna et al. 2012; Kessouri et al. 2019), and ground penetrating radar (GPR) (e.g. Grote et al. 2003; Krueger et al. 2013) have the capacity to assess the soil pore space and how its varied distributions will affect soil hydrology.

Although geophysical methods have the potential to provide the high-resolution understanding of soil spatiotemporal variabilities needed to improve representation of coastal TAIs in ESMs, this approach is yet to be fully explored because most geophysical investigations of soil are focused on purely terrestrial ecosystems. In this study, we combined three geophysical methods (EMI, ERT, and GPR) with borehole information, as well as soil sensor and groundwater data, to characterize soil architectural properties across land-lake interfaces along Lake Erie. This approach provides a non-invasive and detailed characterization of TAI soils at high spatiotemporal resolution, which is usually lacking with point sampling approaches. Combining different geophysical methods is useful to understand both the lateral (using EMI) and vertical (using ERT and GPR) variations in soil properties across the TAI. This approach could precisely direct sampling and monitoring campaigns, replacing haphazard sampling and providing essential data for constraining pedophysical and hydrological models across the TAIs. Here, we used a variety of geophysical techniques to test the hypothesis that soil properties will show both vertical and horizontal heterogeneity across land-lake interfaces.

2. Study Area

Our study sites are situated along the western-central basin of Lake Erie, the fourth largest of the five Great Lakes in North America and the eleventh largest lake globally (Hansen, 1989). Lake Erie is located on the international boundary between the United States and Canada. The northern shore is bounded by the Ontario province of Canada, while the U.S. states of Michigan, Ohio, Pennsylvania, and New York bounds the western, southern, and eastern shores. The three study sites, Crane Creek (CRC), Portage River (PTR), and Old woman creek (OWC) (Figure 1), are located in the North West Ohio portion of the Western Lake Erie Basin (WLEB) which is one of United States' most significant collections of inland rivers and streams. The WLEB covers nearly 7 million acres and stretches across most of northwest Ohio, portions of northeast Indiana, and southeast Michigan. Around 75 percent of the land is used for agricultural production. Approximately 1.2 million people live in the basin, distributed between three urban centers, Toledo, Ohio; Fort Wayne, Indiana; Lima, Ohio, and numerous cities and towns.

The geology of the Lake Erie region is characterized by middle Paleozoic sedimentary rocks composed of limestones, dolomites, shales, and sandstones (Bolsenga and Herdendorf 1993). These rocks were deposited about 430 to 300 million years ago under conditions ranging from tropical barrier reef habitats to deltaic and deepwater clastic environments associated with mountain building (orogenic) episodes and tectonic plate collisions (Herdendorf, 2013). These episodes and the resulting uplifts ushered in a long period of erosion which led to the excavation of deep stream valleys and a mature drainage system along the longitudinal axis of the present lake. Continental glaciers during late Cenozoic Era (Pleistocene Epoch beginning about 2.5 million years ago) further sculpted this valley system by overriding the Niagara Escarpment and excavating most deeply in the shale at the eastern end of the lake, moderately deeply in the shales

of the central portion, and least deeply in the limestone/dolomite bedrock at the western end of the lake, a process that formed three distinctive basins (Western, Central and Eastern basins) that characterize Lake Erie (Herdendorf, 2013). After the most recent glacial advance (Wisconsinan Stage), the ice margin receded in pulses, with several ridges of glacial debris (moraines) being deposited under what is now the bed of Lake Erie (Lewis et al. 2012). Moraines composed mainly of glacial till clay and gravel were built up at the ice margins as advancing or retreating ice sheets paused, which dammed earlier drainage systems at different locations. (Herdendorf and Krieger 1989). The age of the bedrock units in this coastal region ranges from the Silurian Period (416 to 435 million years ago) in western Ohio to the Pennsylvanian Period (307 to 318 million years ago) in the bedrock highland areas (see Figure S1) (ODNR, 2018). Along the Lake Erie shore west of Sandusky, bedrock units exposed at the surface or buried beneath glacial deposits are mostly Silurian and Devonian-age limestone and dolomite (exposed at Catawba, Bass, and Kelleys Islands). East of Sandusky, Devonian-age shale trends along the shore into northeastern Ohio (exposed in the valley walls of the Vermilion, Black, and Rocky Rivers).

The soil parent materials, which refer to the underlying mineral or organic materials from which soil forms, are usually categorized by means of sediment transport e.g., ice, water, wind, and gravity. Myers et al. (2000) and ODNR (2018) classified the soils across the three study sites into Lakebed (lacustrine) soils and glacial till soils based on their parent materials. The Lakebed soils are fine-textured lacustrine deposits usually formed at the lake bottoms and were deposited during the prehistoric stages of Lake Erie's formation (ODNR, 2018). Glacial till soils are unsorted (variable-sized) materials that were mixed, crushed, compressed, and transported by the movement of glaciers. Till soils have variable textures and can be slightly permeable below the

surface. Also, these soils can be classified further into Inceptisols, Alfisols, mollisols, and a small fraction of Entisols based on the dominant soil order (see Figure S2).

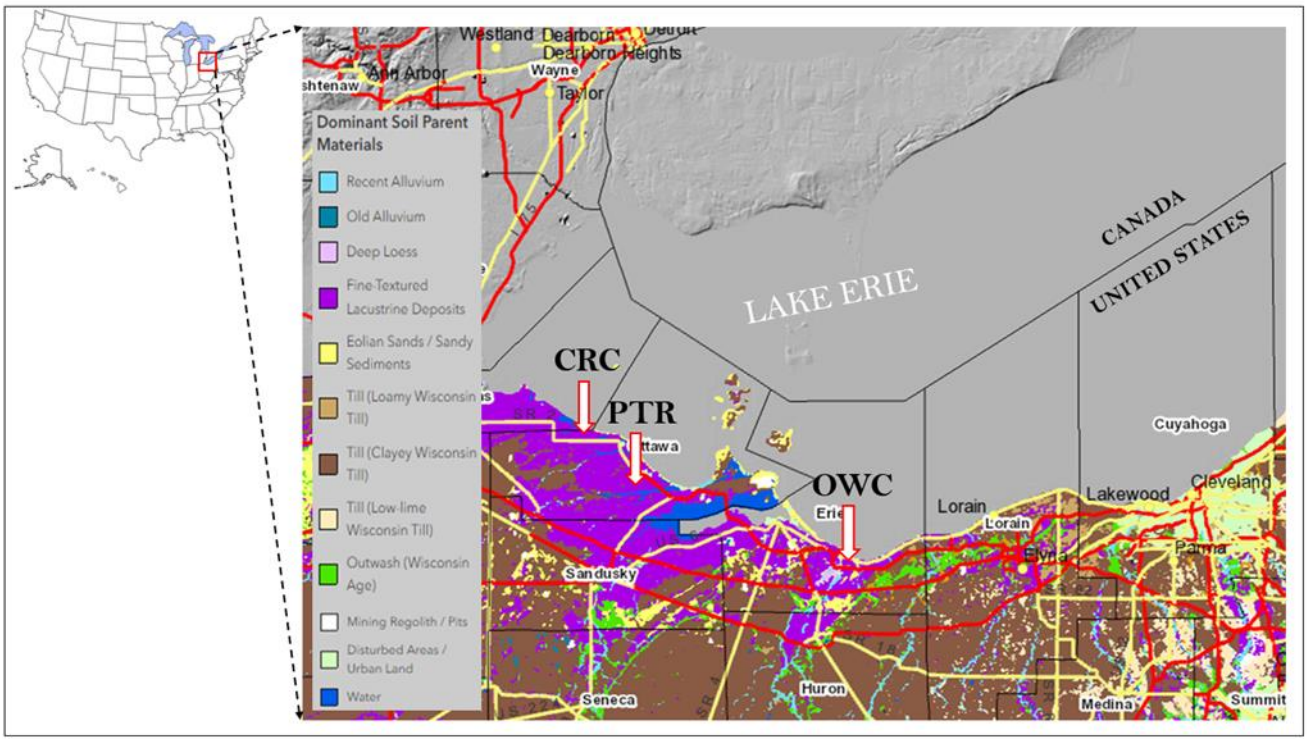

Figure 1. Map of the United States (top left), surficial geologic map of the study area showing the dominant soil parent material overlaid on hillshade basemap (right). Data source: Gridded Soil Survey Geographic Database for Ohio (SSURGO, 2012), with dominant soil parent material overlay by S. Subburayalu and B. Slater (2013).

3. Materials and methods

3.1. Lithostratigraphy

2 inch diameter piezometers were installed at the upland, transition, and wetland zones of each of the three field sites, using a hand auger with soil samples retrieved every 0.1 m. The piezometers were deeper at the upland zones terminating at about 6 m, while the transition and wetland piezometers terminated at about 2 m and 1 m, respectively. The soil samples retrieved during

198 piezometer installation were used to create lithostratigraphic logs that were used to ground-truth
199 some of the geophysical measurements.

200 **3.2. Electromagnetic Induction**

201 The EMI method measures the response of the ground to the propagation of Electromagnetic
202 fields made up of an alternating electric intensity and magnetizing force. An alternating current is
203 passed through a transmitter coil (a loop of wire) placed over the ground to generate a primary
204 (inducing) magnetic field which spreads out both above and below the ground surface. In a
205 homogeneous ground, the primary field is detected by a receiver coil with a minor reduction in
206 amplitude (Haldar, 2018). In the presence of a conducting body, however, the magnetic
207 component of an electromagnetic field penetrating the ground induces the flow of eddy currents
208 within the conductor. The eddy currents generate their own secondary electromagnetic field,
209 which differs in phase, amplitude, and direction, sensed by the receiver coil. The differences
210 between transmitted and received electromagnetic fields reveal the presence of a conductor and
211 provide information on its geometry and electrical properties (Geonics, 2009; Gebers et al. 2009).
212 For this study, EMI data was acquired with an EM38-MK2 sensor (Geonics, Canada). The sensor
213 consists of a transmitter and two receiver coils at separation distances of 0.5 m and 1.0 m from
214 the transmitter and outputs apparent electrical conductivity (ECa) at average depth ranges of 0-
215 0.75 m and 0-1.5 m in vertical mode and 0-0.38 m and 0-0.75 m in horizontal mode. However,
216 the true penetration depth of the sensor depends on the sensor frequency and conductivity of the
217 topsoil, which is site-specific (e.g., Paton, 2012). The sensor operates at a frequency of 14.5 kHz
218 and delivers ECa values in mS/m.

219 In this study, the EM38-MK2 sensor was used in vertical mode to pace around each site with a
220 back-mounted real-time kinematic differential ground positioning system (RTK-DGPS). The

RTK-DPS system was set up using two Emlid Reach RS2+ differential GPS (Emlid Ltd., Hong Kong), one was fixed at a location that serves as the base while the other was mounted on a backpack and serves as the rover, this allowed the acquisition of a georeferenced data at about 0.3 m accuracy. The data acquisition was monitored real-time using EM38-MK2win data logging system operated on a Windows 10 based field tablet computer. The EMI system was nulled and calibrated at each site before data acquisition, and the sensor was held up at about 0.4 m from the ground during acquisition. The acquired ECa data was interpolated with Surfer 12 (Golden Software, Colorado, USA), using inverse distance to a power approach (Franke, 1982), resulting in a spatially distributed ECa. At the CRC transition and wetland zones, measurements were repeated in December 2022 and April 2023 to investigate the temporal variability of the soil ECa.

3.3. Electrical resistivity tomography

Electrical resistivity tomography is used to determine the subsurface distribution of electrical resistivity by carrying out a set of resistance measurements on the ground surface and/or in boreholes. Current is injected into the ground via two current electrodes, and the resulting potential difference is measured at another two electrodes using different combinations of current and potential electrodes along a transect or grid. A geophysical inversion of the acquired data is then performed to obtain the resistivity of the subsurface (see Loke, 2000). In this study, ERT data were collected across the three sites with a SuperSting R8 resistivity meter and an 84-electrode switch box (Advanced Geosciences Inc., Austin, TX), using the dipole-dipole electrode configuration (e.g. Loke, 2000) and 1 m unit electrode spacing. The data was collected in automatic mode, which automatically records resistivity data using a preprogrammed command file and the distributed Swift automatic multi-electrode system (AGIUSA, 2005). At the CRC site, ERT data were collected along 3 transects in the upland zone and another 3 transects between the transition and wetland zones. At the PTR site, six different transects were used to

acquire ERT data. The two longest profiles were acquired using a roll-along method up to a total spread of 147 m from the transition zone to the wetland zone, and 168 m from the upland zone to the wetland zone, while the other four transects were 84 m long. The ERT data at the OWC site were acquired along 7 different transects cutting across the three zones, thus, a total of 19 resistivity profiles were obtained across the three sites. The ERT survey was designed in such a way as to enable a correlation of electrical resistivity with the lithostratigraphic logs obtained from the piezometers installed in each of the sites. The inversion of the acquired resistivity data was performed with the AGI EarthImager 2D (Advanced Geosciences Inc., Austin, TX) using smoothness constrained inversion method. Finally, the Earth Imager was used to trim the ERT profiles to a depth suitable for high-resolution correction to be made with the well logs.

3.4. Ground penetrating radar

Ground penetrating radar is a geophysical method that uses propagating electromagnetic waves to investigate the shallow subsurface based on its response to changes in the electromagnetic properties of the shallow subsurface. The propagation wave velocity is determined by the relative permittivity contrast between different soil layers or the background material and anomalous body (e.g., Baker et al., 2007). The transmitter component of the GPR system propagates the electromagnetic wave through the earth material and the interactions with the earth material response are sensed by the receiver component. The GPR survey in this study was carried out on short survey lines, collocated on some of the ERT survey lines in each site to allow the comparison of both methods in terms of suitability for investigating vertical variations and delineating subsurface heterogeneity at the land-lake interface. GPR data were collected using PulseEKKO GPR system (Sensors & Software Inc., Canada) with a 200 MHz antenna. Transmitter and receiver separation of 0.5 m was used, and the GPR data was collected at 0.5 m

intervals using a manual trigger method. The new DVL-500 ruggedized display unit (a high-visibility touchscreen) was used to visualize the data simultaneously during acquisition.

The acquired data were processed using Sensor & Software's EKKO_Project, following standard GPR processing for subsurface characterization (e.g., Annan, 2009), to remove low-frequency noise due to inductive coupling effects and /or dynamic range limitations of the antennas (Annan, 2009).

3.5. Soil and groundwater measurements

Teros 12 soil sensors, which measure soil moisture, temperature, and electrical conductivity (Meter Group, Inc. USA), were installed at 10 and 30 cm depth in the upland (n=4 and 2, respectively), transition (n=4 and 2, respectively), and wetland (n=2 and 2, respectively) zones of each site and were used to monitor monthly soil moisture (SM) changes between March 2022 and April 2023.

Also, each piezometer was instrumented with Aqua TROLL 600 multiparameter sondes (In-situ Inc. USA), which were used to measure monthly changes in groundwater level and specific conductivity. The sensors were equipped with wipers to minimize fouling of sensor heads and calibrated according to manufacturer protocols during maintenance visits. The soil and groundwater sensors were both set to log data on a 15-minute frequency.

4. Results

4.1. Spatial variability of soil properties from apparent electrical conductivity

The range, mean, and variance of soil apparent electrical conductivity (ECa) measured at the three sites are described in Table 1. The sites show high spatial variability in the ECa distribution from the 0.5 m and 1.0 m sensor separation, corresponding to average depths of 0-0.75 m and 0-1.5 m, respectively (Figure 2). Also, the ECa values showed Gaussian distribution across all sites,

with higher values in the wetland and transition zones than the upland zones for the PTR and OWC sites. The CRC upland showed higher ECa values at 0.5 m (mean = 55.3; variance = 0.041) and 1.0 m (mean = 49.3; variance = 0.012) sensors separation than the CRC transition and wetland at 0.5 m (mean = 12.8; variance= 0.004) and 1.0 m (mean = 28.7; variance = 0.006) sensors separation. The ECa values across the sites are generally higher at the 1.0 m coil separation than at 0.5 m (see Table 1), but again the CRC upland showed an opposite behavior with higher ECa values at the 0.5 m sensor separation (Figure 2a, Table 1)). The CRC transition and wetland zones also showed lower ECa values compared to OWC and PTR wetland and transition zones.

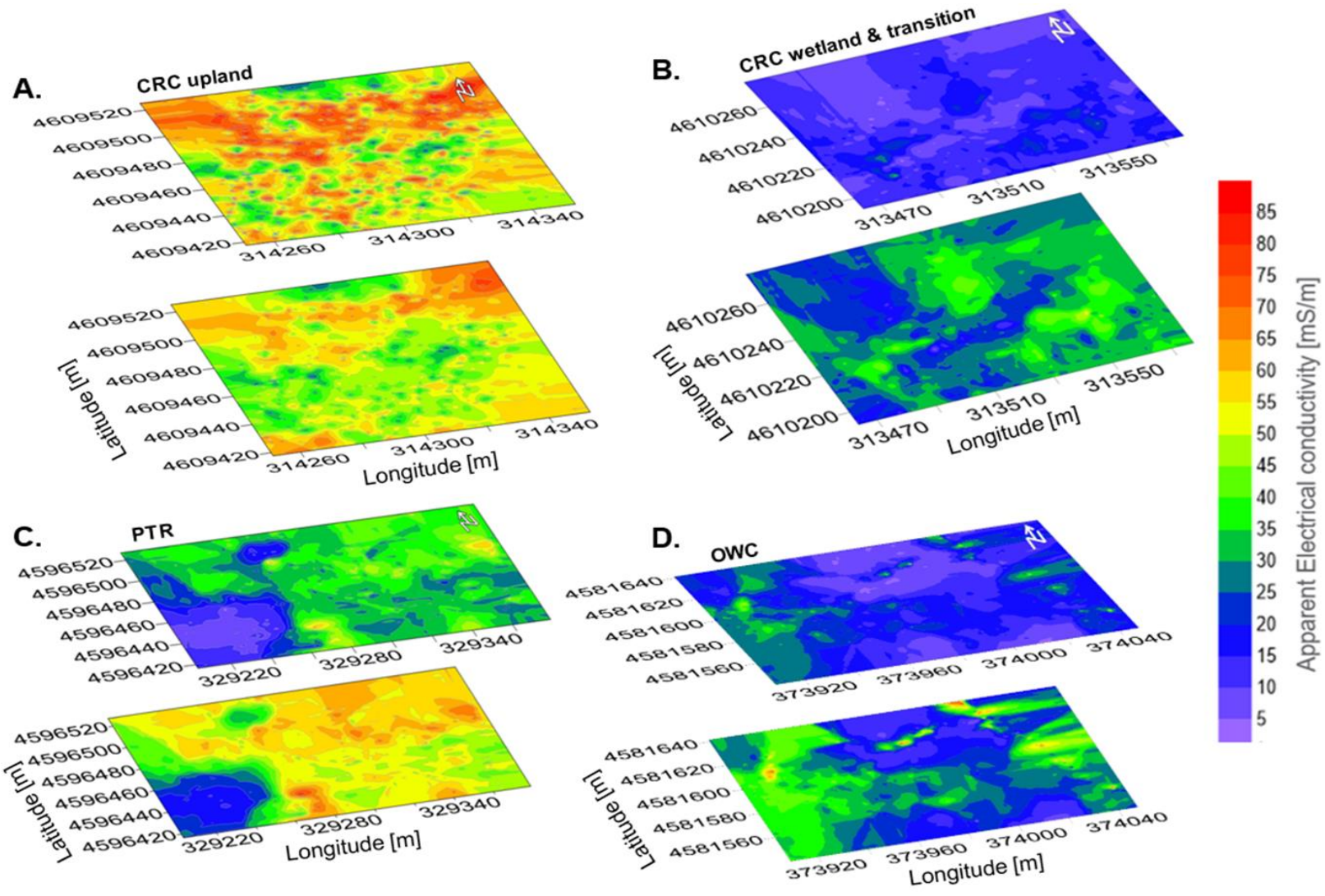
A.
CRC upland
B.
CRC wetland & transition
C.
PTR
D.
OWC
N
Latitude [m]
Longitude [m]
4609520
4609500
4609480
4609460
4609440
4609420
314260
314300
314340
4610260
4610240
4610220
4610200
313470
313510
313550
4596520
4596500
4596480
4596460
4596440
4596420
329220
329280
329340
4581640
4581620
4581600
4581580
4581560
373920
373960
374000
374040
Apparent Electrical conductivity [mS/m]
85
80
75
70
65
60
55
50
45
40
35
30
25
20
15
10
5

300

Figure 2. Apparent electrical conductivity (ECa) distribution maps of the sites (a) CRC upland, (b) CRC wetland and transition, (c) PTR, and (d) OWC, at transmitter-receiver spacing of 0.5 m (top) and 1.0 m (bottom) which correspond to approximate depth of 0-0.75 m and 0-1.5 m respectively.

304 **Table 1** The ECa distribution across the study sites at 0.5 m and 1.0 m coil spacing

Site	ECa distribution at 0.5 m coil separation [mS/m]	ECa distribution at 1.0 m coil separation [mS/m]	Comments
CRC upland	Range: 4.5 - 85 Mean: 55.3 Variance: 0.041	22.7 - 77.9 Mean: 49.3 Variance: 0.012	- ECa is higher and more variable at top 0.5 m coil spacing - Higher ECa values than the other uplands
CRC wetland and transition	Range: 1 - 36.7 Mean: 12.8 Variance: 0.004	Range: 7.2 - 53.4 Mean: 28.7 Variance: 0.006	- ECa is higher and more variable at 1.0 m spacing
PTR	Range: 2.6 - 63.8 Mean: 31.2 Variance: 0.17	Range: 12.9 -77 Mean: 49.4 Variance: 0.020	- ECa is higher and more variable at 1.0 spacing m coil spacing - Lower ECa values in the upland
OWC	Range: 2 - 52 Mean: 17.9 Variance: 0.17	0.9 - 85 Mean: 27.9 Variance: 0.19	- ECa is higher and more variable at 1.0 m coil spacing - Lower ECa values in the upland

305

306

307 **4.2. Soil ECa patterns compared to traditional soil maps**

308 Previous works have recommended that ECa maps be used to optimize soil mapping (e.g.,
309 Corwin and Lesch, 2003; Mertens et al. 2008). Soil ECa maps are compared to traditional soil
310 maps from the United States Department of Agriculture (USDA), as shown in Figure 3. A closer
311 match between the USDA soil maps and the soil ECa maps was observed at CRC upland and
312 OWC sites than for PTR and CRC wetland and transition. Generally, the ECa maps revealed soil
313 units that were identified from the USDA soil maps, and also revealed the presence of minor
314 subunits that were not captured in the traditional soil maps (Figure 3). At the CRC site, Toledo

315 silty clay (To), Toledo silty clay, ponded (Tp) and Nappanese silty clay loam (NpA) were the
316 three major soil units identified from the USDA soil map (Figure 3a), both *To* and *Tp* are hydric
317 soils with 0-1 % slope while NpA is a non-hydric soil with 0-3 % slope. The hydric soil units *Tp*
318 and *To* showed higher ECa values than the non-hydric *NpA* soil unit. The ECa maps provided a
319 more precise detail of the lateral extension of each of these soil units than the soil map and
320 identified additional subunits that were missing in the soil map (see supplementary Table 1). At
321 the CRC wetland and transition, the USDA soil map placed the site in one soil unit (*Tp*), while
322 the ECa map showed a clearer lateral variation indicating the presence of additional units/sub-
323 units (Figure 3b). The PTR soil map showed only the *To* and *Tp* soil units (Figure 3c), with the
324 ECa values higher in *Tp* than the *To,* as was also the case at CRC upland site. The ECa map at the
325 PTR site showed a more precise lateral extent of the *Tp* and *To* soil units and also indicated the
326 presence of additional units/sub-units which were missed out in the soil map (supplementary
327 Table 1). At OWC, the soil map showed three distinct soil units which were clearly identified by
328 the ECa maps (Figure 3D), the Zurich silt loam (*ZuF*), which is rated non-hydric with 25-40%
329 slope, Holly silt loam (*HoA*) which is rated hydric with 0-1 % slope (Hurt and Vasilas, 2006), and
330 Del Rey silt loam (*DeA*), a nearly level and somewhat poorly drained soil with 0-2 % slope. The
331 hydric *HoA* soil unit showed higher ECa values than the non-hydric units.

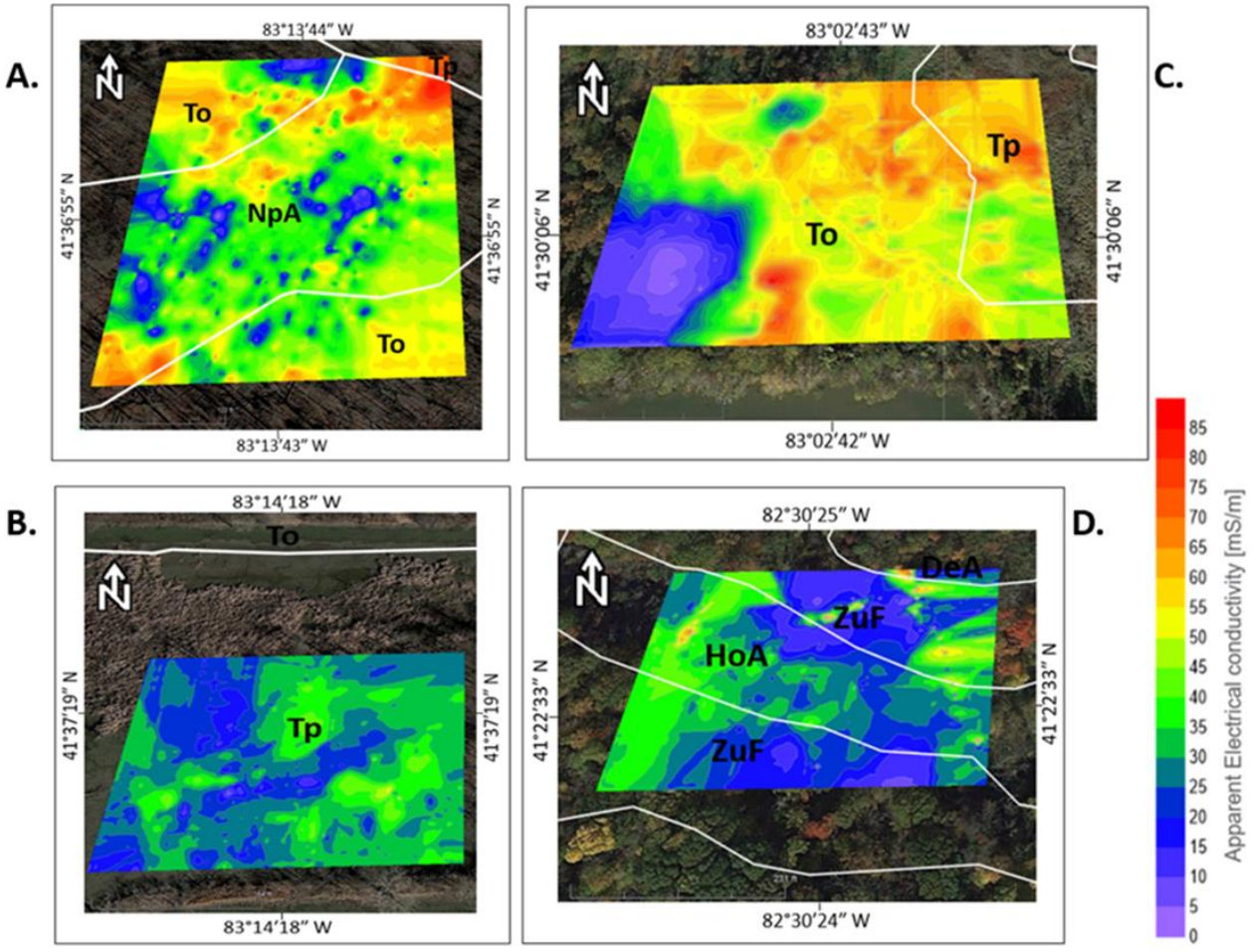

Figure 3. An overlay of soil ECa distribution from 1.0 m spaced sensors on USDA soil maps. (a-b) CRC upland and CRC transition and wetland showing three soil units; Toledo silty clay (To), Toledo silty clay, ponded (Tp) and Nappanese silty loam (NpA). (c) PTR showing two soil units; Toledo silty clay (To) and Toledo silty clay, ponded. (d) OWC showing three soil units, Zurich silt loam (ZuF), Holly silt loam (HoA) and Del Rey silt loam (DeA).

4.3. Soil moisture and groundwater dynamics

Figure 4 shows the in situ Soil moisture, temperature, and electrical conductivity (EC) data obtained from the CRC upland, transition and wetland zones. At the wetland zone, the SM increased slightly from 0.52-0.55 m^3m^{-3} at 10 cm depth, and from 0.45-0.46 m^3m^{-3} at 30 cm depth between December 2022 and April 2023. At the transition zone, the SM also increased between December 2022 and April 2023, and the values ranged from 0.26-0.32 and 0.46-0.50

344 m^3m^{-3} at 10 cm depth, and from 0.30-0.40 and 0.41-0.44 m^3m^{-3} at 30 cm depth (Figure 4c). The
345 changes in soil moisture were much more variable at the top 10 cm. During the same period, we
346 recorded a substantial increase in soil electrical conductivity from about 10-750 uS/cm and 500-
347 1000 uS/cm in the transition and wetland zones, respectively (Figure 4a), the soil temperature
348 was also close to 0° C as shown in Figure 4b.

349 The specific conductivity of groundwater at the CRC transition zone from August to September
350 2022 and from April-May 2023 is shown in Figures 5a and 5B, respectively. In August 2022, the
351 specific conductivity decreased with the hydraulic head (Figure 5a). The water level in the
352 piezometers continued to decrease until it dried up in October-December 2022 (no data
353 recorded). In the same period, our results show a decrease in both soil moisture (Figure 4c) and
354 soil electrical conductivity (Figure 4a), while the soil temperature increased from April and
355 peaked in August before decreasing to a minimum around December for both transition and
356 wetland zones (Figure 4b). In April 2023, the specific conductivity showed a steady increase with
357 the hydraulic head (Figure 5b).

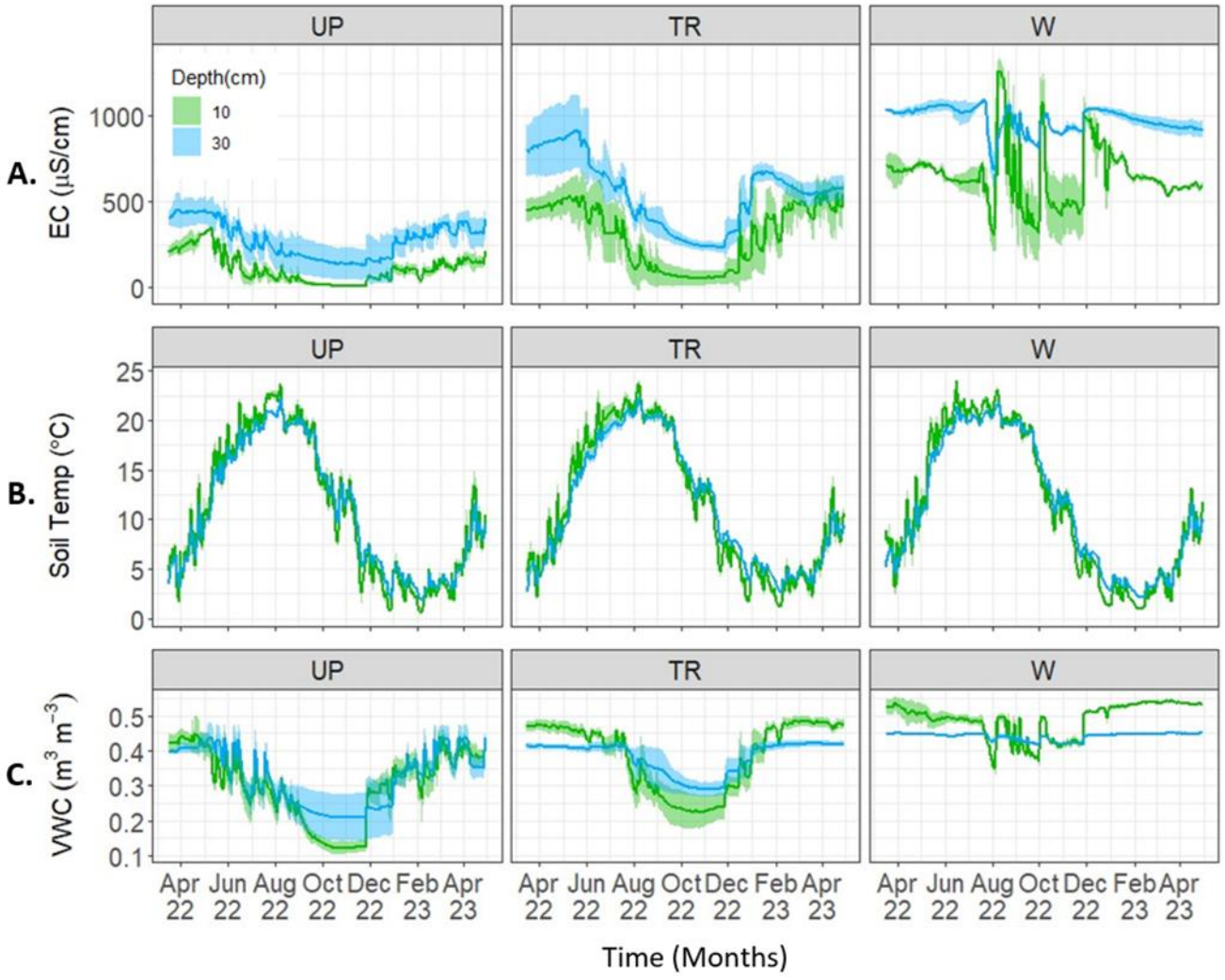

Figure 4. (a) Soil electrical conductivity (EC), (b) temperature and (c) moisture changes recorded between April 2022 and April 2023 at CRC upland zone (UP), transition zone (TR) and wetland zone (W).

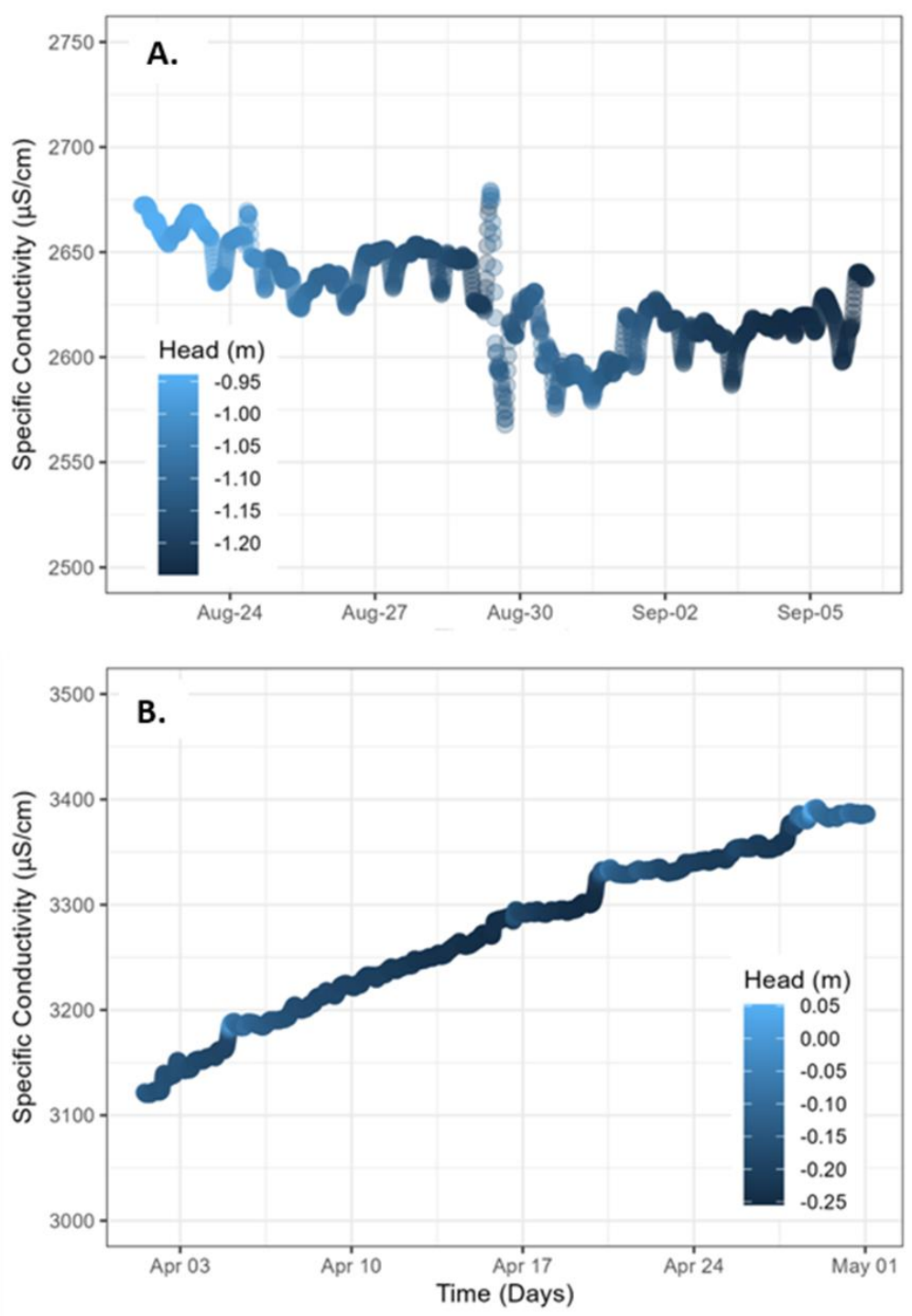

Figure 5. Specific conductivity and hydraulic head variations recorded in (a) August 2022 and (b) April 2023, at the CRC transition zone.

4.4. Vertical variability of soil properties assessed from ERT and GPR

The ERT results show a vertical variation in electrical resistivity, generally increasing from the soil surface to 19.7 m across the three sites, as shown in Figure 6. The CRC site showed resistivity values that ranged from 5.1-54.4 Ωm and 10.4-70 Ωm for the upland and wetland-transition zones, respectively (Figure 6 a-b). A low resistivity layer is clearly visible at the depth of 1.3-6 m in the upland and 0-3 m in the transition and wetland zones. At the PTR site, the resistivity ranged from 5.5-74 Ωm (Figure 6d), with low resistivity values from the soil surface to a depth of about 6 m in the transition zone and about 3 m in the wetland zone. In the upland zone, higher resistivity values are observed from 0-1.6 m depth. The OWC showed a more variable resistivity response, which ranged from 10.2-148 Ωm (Figure 6c), high resistivity values were observed in the upland but also in the transition and wetland at shallower depths compared to the CRC and PTR sites. While the CRC and PTR sites are generally flat, the OWC site shows significant elevation differences between the upland zone and the wetland or transition zone. The ERT profiles 2 and 3, which extended from the wetland into the upland, were corrected for terrain effect during inversion.

At the CRC transition (Figure 7a), three distinct stratigraphic layers were identified from the GPR reflection radargram. Layer 3 showed stronger reflection compared to layers 1 and 2. Similarly, three stratigraphic layers were also identified at the PTR site, on a transect which extended from the upland zone to the wetland zone (Figure 7b). There is a visible lateral change in GPR reflection at about 45 m mark along the profile, which signifies the boundary between upland soil (1) and wetland soil (2) as described in Figure 7b. There are also some vertical features that appeared at 10 m and 60-70 m along the profile and extended to an estimated depth of about 3-3.5 m, which are probably a strong reflection of till, as the soil samples retrieved from piezometer installation in this zone confirmed that the till here is very rich in pebbles (diamictites) composed

391 mainly of black shale. At the OWC site, two distinctive layers were observed. A top layer (1) of
392 about 0.5 m thickness which showed a weak reflection and a second layer (2) with a stronger
393 reflection which lies between 0.5-1.5 m. The GPR data is useful to identify the stratigraphic
394 boundaries at these sites but does not reveal what the structures are. Combining different
395 geophysical methods is useful to overcome this challenge by leveraging the strength of each
396 method to bridge the gap in interpretation where other methods are lacking. Thus, the GPR
397 results will be compared with other methods to better identify the observed layers and structures
398 (see section 4.6).

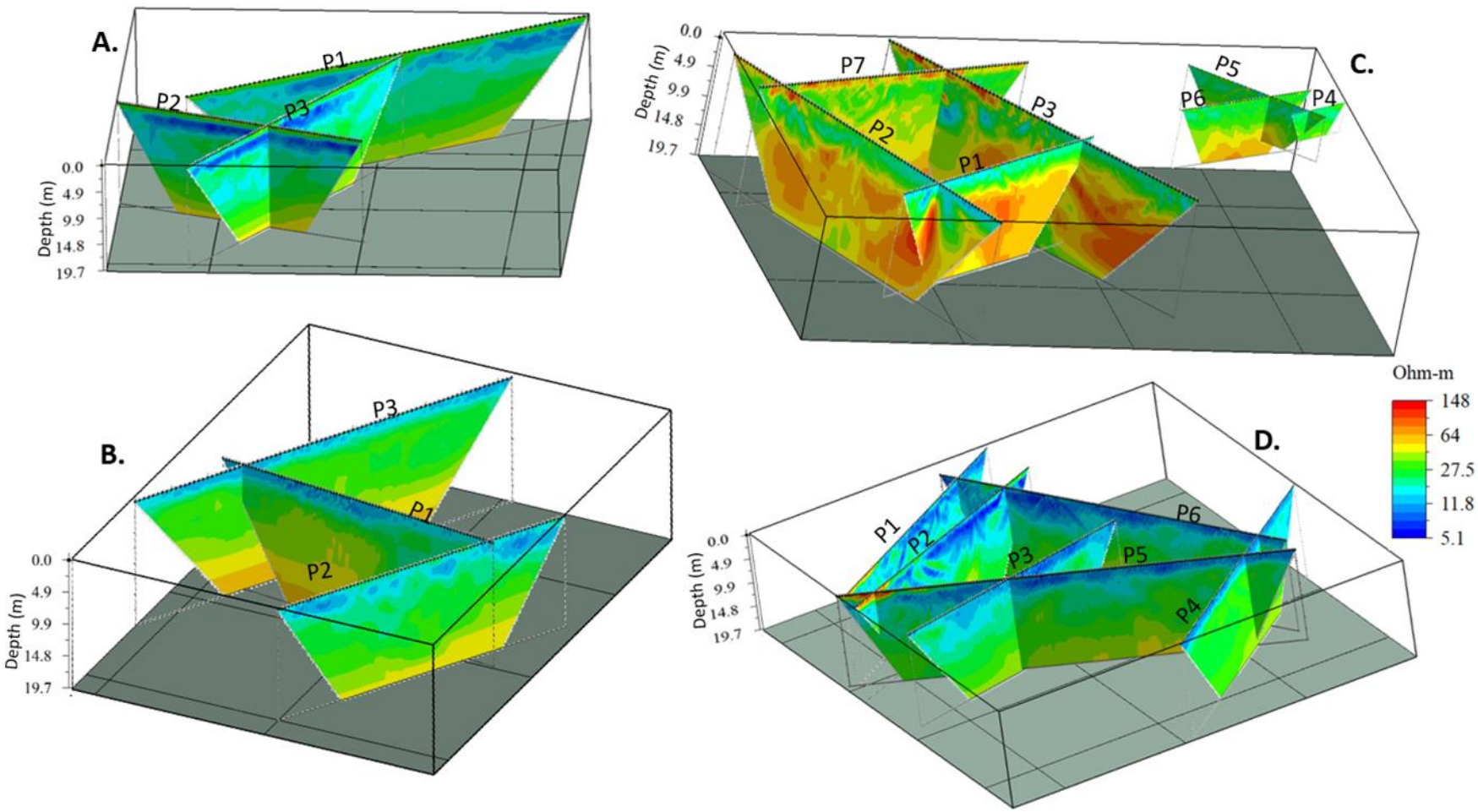

Figure 6. Electrical resistivity tomography profiles from the sites. (a) CRC upland (b) CRC transition and wetland (c) OWC site (d) PTR site. For clarity, the profiles in each zone are numbered as P1, P2...Pn., according to the sequence of acquisition.

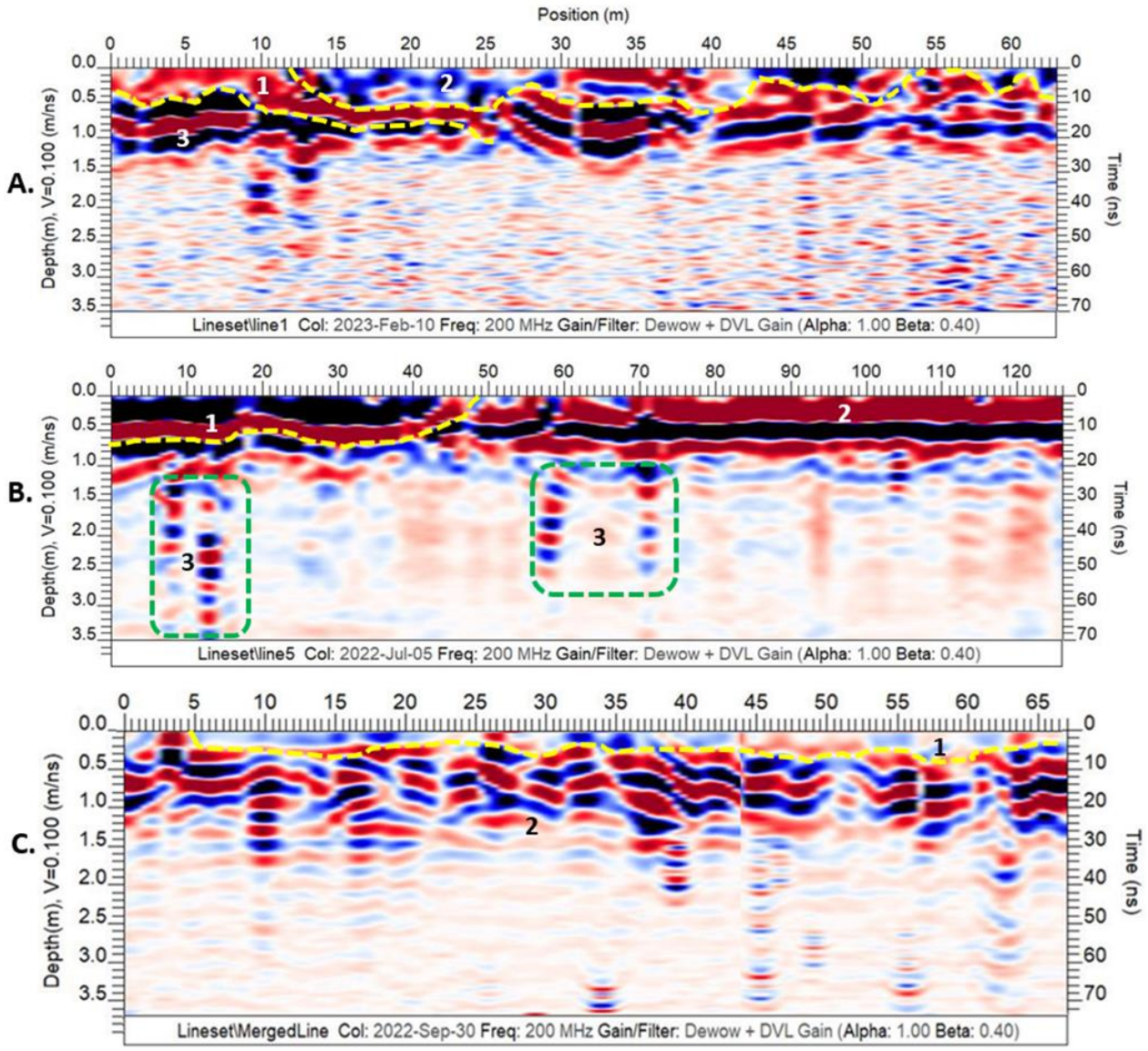

Figure 7. Ground penetrating radar profiles from the sites (a) CRC transition zone (b) PTR upland to wetland zone (c) OWC wetland edge to wetland center. The numbers on the figures indicate the different layers identified from the GPR reflection, while the yellow and green lines are used to mark the layer boundaries.

4.5. Lithostratigraphy reconstructed from well logs

The lithostratigraphy of the three sites is described here based on the borehole logs obtained from the upland, transition, and wetland zones of each site (Figure 8). The CRC and PTR upland zones are characterized by silty clay layers at the top 1.7 m, underlain by clay with intercalations of

412 black shale and claystone (glacial till) which extends down to 5.5 m. The CRC transition zone
413 shows similar stratigraphy with the CRC upland, while the PTR transition zone is different from
414 the upland, it shows a layer of silty clay which extends down to 0.5 m followed by a clay layer
415 down to 2 m. The OWC upland zone is characterized by a thin layer of silty loam at the top 6 cm,
416 followed by a clay layer extending down to 1.35 m, then a silty clay from 1.35 to 4.0 m, followed
417 by water-saturated clay from 4-5.8 m. The wetland zones of the three sites show similar
418 stratigraphy characterized by a 1 m thick clay layer.

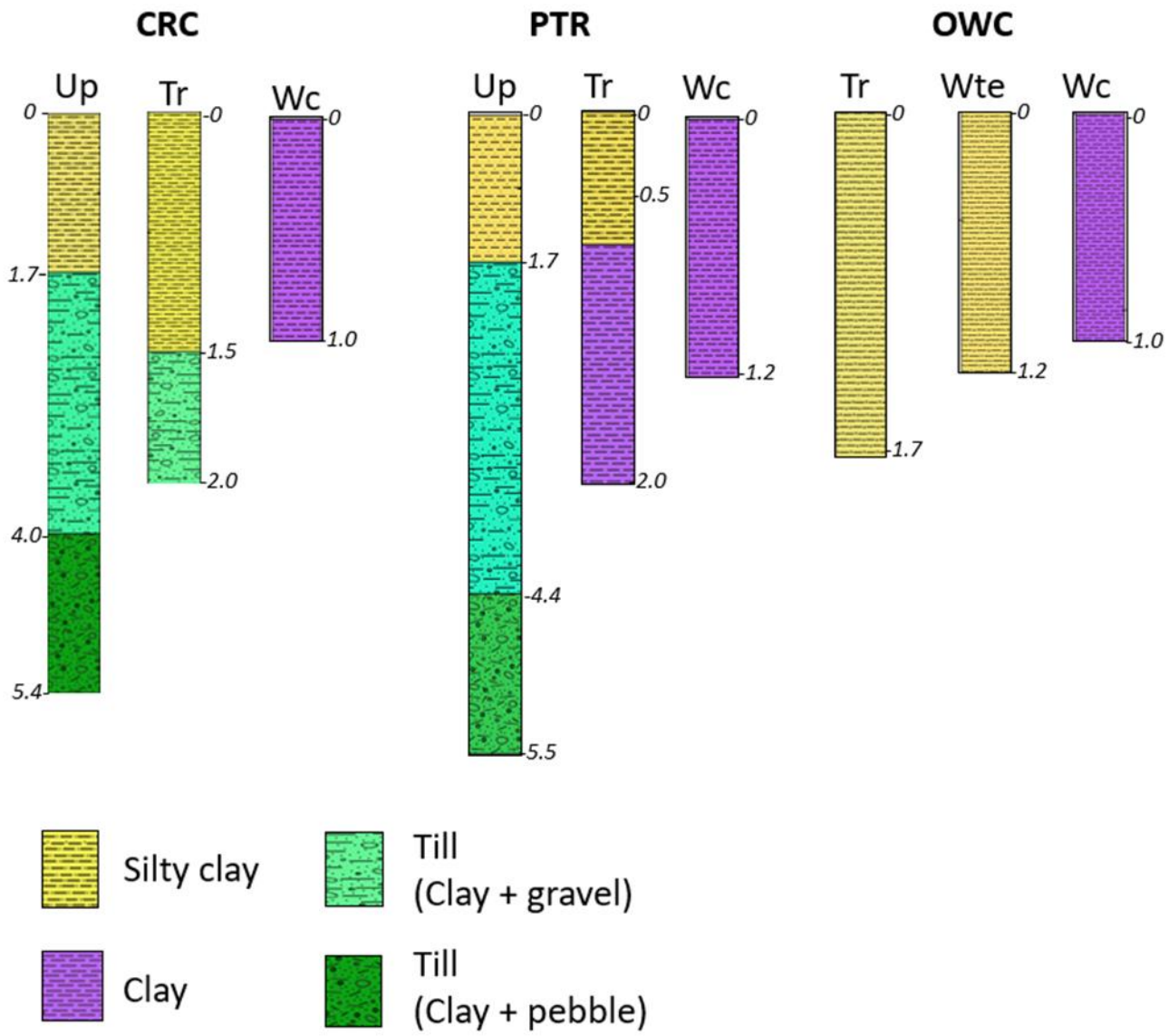

Figure 8. The lithostratigraphy of the sites described based on borehole logs from the upland zones (Up), the transition zones (Tr), wetland edge (Wte) and wetland center (Wc) of the three sites, with depth in meters.

4.6. Combining ERT, lithological logs and GPR

At the CRC site, the upland well was correlated with two ERT profiles that cut across the well at different positions (Figure 9a-b). The stratigraphic boundaries observed in the well-log matched that of the ERT profiles. The well log identified a sharp boundary in the till layer marked by a

different clay-to-rock fragment ratio; this boundary was also observed in the ERT profiles (Figure 9a-b). The low resistivity layer in the upland is tied to the till, while the higher resistivity layer is tied to the silty clay layer. In the transition and wetland zones, the stratigraphic boundaries observed in the wells also matched that of the ERT profiles taken across them (Figure 9c-e). Figure 9c showed a transect from the wetland zone to the transition zone, the well log and ERT result identified a shift from clay-dominated top layer in the wetland to silty clay-dominated top layer in the transition zone. The Till layer appeared deeper in the wetland zone (Figure 9e) compared to parts of the transition zone (Figure 9d).

At the PTR site, the upland well log was tied to two ERT profiles (Figure 10a and 10d). The stratigraphic boundaries observed from the well log also matched that of the ERT profiles very closely; the high resistivity layer observed from the ERT profile was confirmed to be a layer of dry silty clay. The transition well log was tied to an ERT profile that ran from the upland zone into the transition zone (Figure 10b) and another that ran from the transition zone into the wetland zone (Figure 10e). The top layer of silty clay identified from the well log clearly matched the ERT result. In the wetland zone, both the ERT profile and the well log identified a top layer of clay. Since the wetland well is just 1 m deep, it was not possible to determine the thickness of this clay from the well log, but the ERT profile showed the thickness to be between 2.5-3.2 m in the wetland zone.

At the OWC site, ERT profiles were correlated with the wells existing in the transition and wetland zones. The transition zone showed relatively uniform resistivity at the top 3 m which is tied to a silty clay layer based on the well log obtained at 2 m depth (Figure 11d). The wetland edge also showed a less heterogeneous layer at the top 3 m which is tied to silty clay as well based on well log data (Figure 11a and 11c). The wetland center showed lower resistivity

response compared to the transition zone, this low resistivity unit was found to be a wet clay layer when tied to the well log obtained at 1 m depth (Figure 11a-b). These results indicate that the stratigraphy and soil moisture dynamics are the key drivers of spatial heterogeneities at these sites.

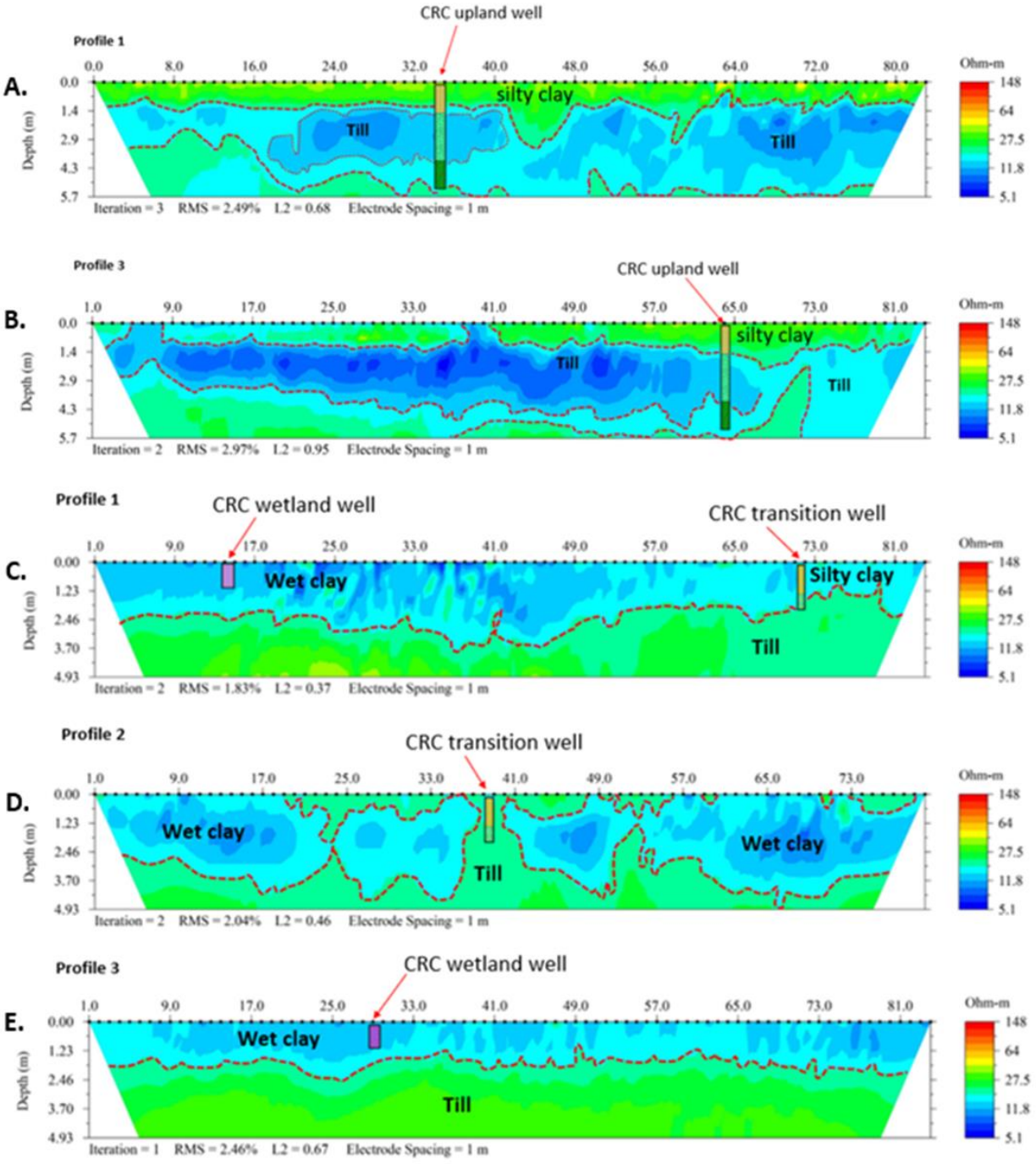

457 **Figure 9.** Correlation of well log and ERT profiles at the Crane creek (CRC) site, showing a
458 close match between stratigraphic boundaries from well logs and that of ERT. (a-b) The dark
459 blue and light blue layers indicate two distinct layers of till identified at CRC upland, the dark
460 blue till layer is clay-rich while the light blue is gravel-rich. (c-e) The till layer at CRC transition
461 zone is composed of more gravel than clay and thus showed higher resistivity than the
462 surrounding wet clay. The existing well at CRC wetland is not deep enough to get into the till.

463

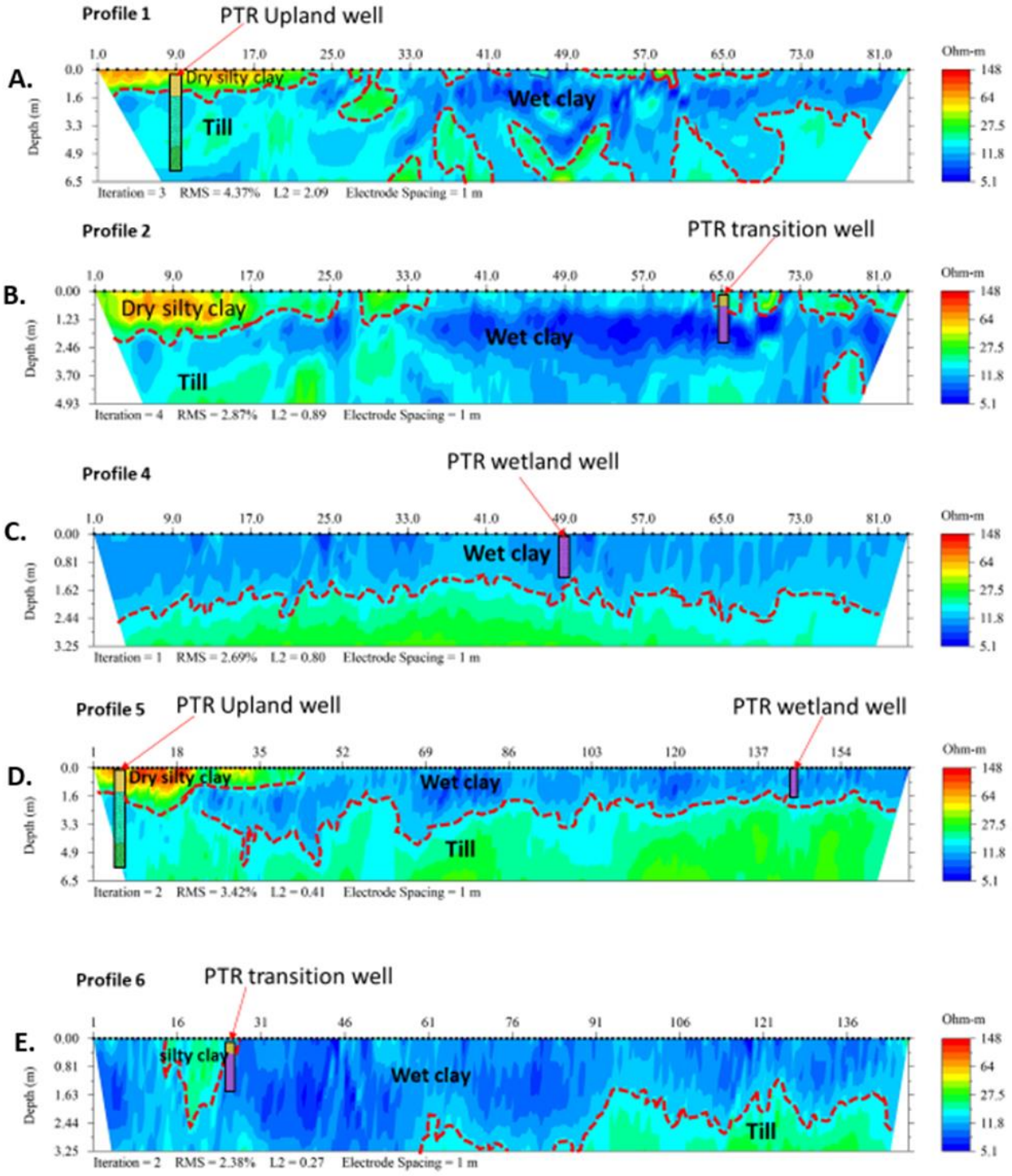

Figure 10. Correlation of well log and ERT profiles at the Portage River (PTR) site. The stratigraphic boundaries observed from the well logs matched that of the ERT, showing dry silty

clay in the upland zone as the most resistive layer (a, b and c), and wet clay in the transition and wetland zones as the least resistive (a-e)

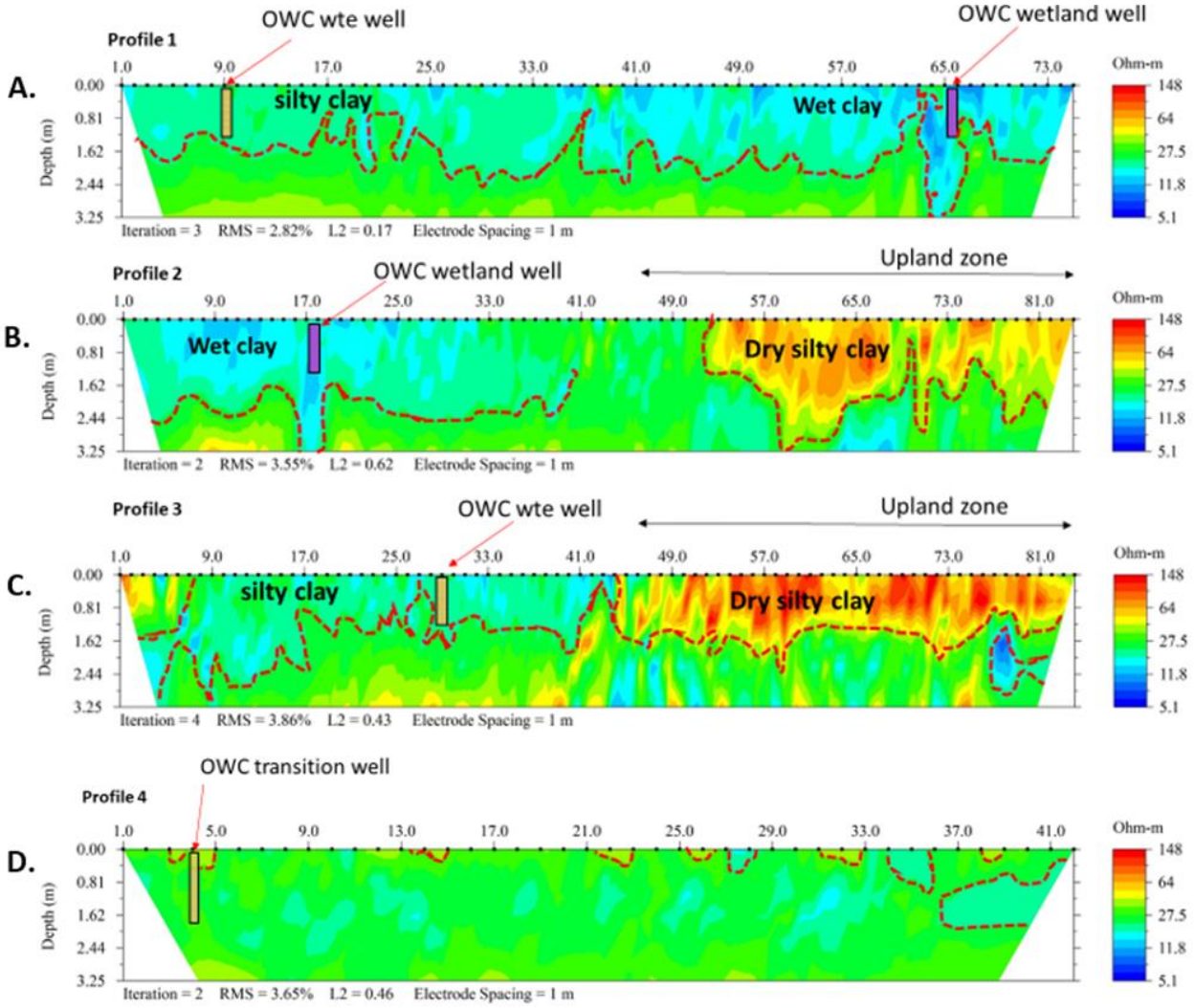

Figure 11. Correlation of well logs and ERT profiles at the Old woman creek (OWC) site, showing wet clay layers in the wetland zone as the least resistive (a-b) and the dry silty clay layer in the upland as the most resistive (b-c).

Figure 12 shows a comparison between collocated ERT and GPR profiles, it is clear that GPR also provided information about vertical variability of soil properties at the study sites. However, the GPR sensitivity at these sites is limited to the top 1.5 m, probably due to signal attenuation due to conductive losses resulting from the high clay content at these sites, while the ERT clearly

479 showed better depth resolution. Correlating the GPR results (Figure 7b) and ERT results (Figure
480 10d) was useful to confirm that the vertical features observed in the GPR just below the dry silty
481 clay are glacial Till (Figure 12b), this clearly shows that combining different geophysical
482 methods is a better approach for subsurface characterization than using one method alone.

483

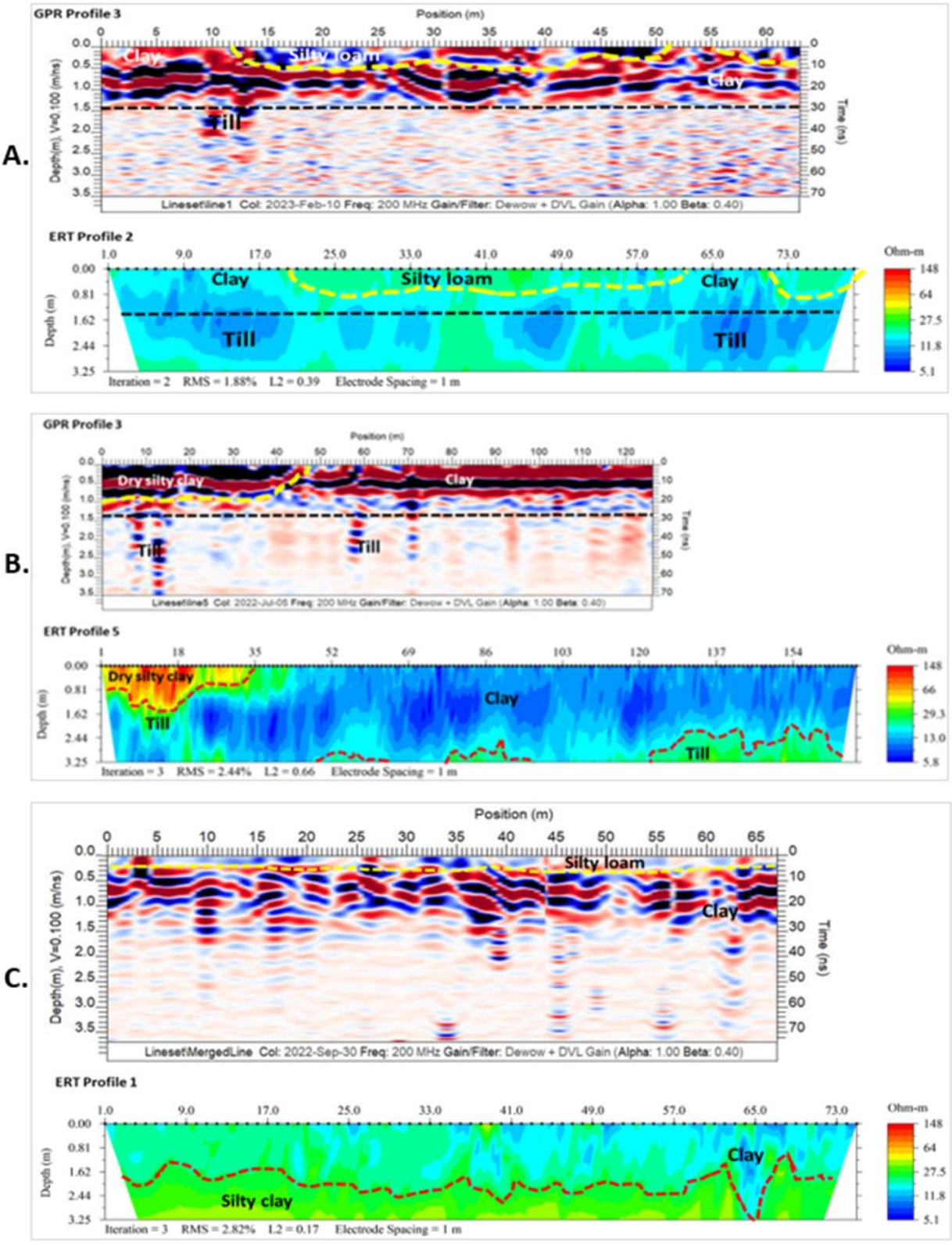
A.
GPR Profile 3
Position (m)
Clay
Silty loam
Clay
Till
Depth(m), V=0.100 (m/ns)
Time (ns)
Lineset\line1 Col: 2023-Feb-10 Freq: 200 MHz Gain/Filter: Dewow + DVL Gain (Alpha: 1.00 Beta: 0.40)
ERT Profile 2
Clay
Silty loam
Clay
Till
Till
Depth (m)
Ohm-m
Iteration = 2 RMS = 1.88% L2 = 0.39 Electrode Spacing = 1 m
B.
GPR Profile 3
Position (m)
Dry silty clay
Clay
Till
Till
Lineset\line5 Col: 2022-Jul-05 Freq: 200 MHz Gain/Filter: Dewow + DVL Gain (Alpha: 1.00 Beta: 0.40)
ERT Profile 5
Dry silty clay
Clay
Till
Till
Depth (m)
Ohm-m
Iteration = 3 RMS = 2.44% L2 = 0.66 Electrode Spacing = 1 m
C.
Position (m)
Silty loam
Clay
Depth(m), V=0.100 (m/ns)
Time (ns)
Lineset\MergedLine Col: 2022-Sep-30 Freq: 200 MHz Gain/Filter: Dewow + DVL Gain (Alpha: 1.00 Beta: 0.40)
ERT Profile 1
Clay
Silty clay
Depth (m)
Ohm-m
Iteration = 3 RMS = 2.82% L2 = 0.17 Electrode Spacing = 1 m

484

Figure 12. Comparing collocated ERT and GPR profiles at (a) CRC transition, (b) PTR upland to wetland transect, (c) OWC wetland edge to wetland center transect. Combining the GPR and ERT methods helped to clearly identify the clay, silty loam, silty clay and till layers.

5. Discussion

5.1. Spatiotemporal variation of soil properties

We hypothesized that ECa will be low in the upland zones and increase as we move from the upland to the transition zone, and from the transition to the wetland zone across the sites due to increasing SM. The EMI results from PTR and OWC agreed with our hypothesis (Figure 2c and 2d), but higher conductivity was observed at the CRC upland (Figure 2a) compared to its transition and wetland (Figure 2b). This is probably due to the temporal variability of SM at the sites considering that the upland area is a separate plot from the wetland and transition, and the EM measurements were conducted at different periods; December (upland) and April (transition and wetland). When this data was compared with the monthly soil moisture data measured at the sites between April 2022 and April 2023, it was seen that SM is higher in April than in December (Figure 4a-b). This should have resulted in higher ECa values in April compared to December but this was not the case as supplementary Figure 3 is showing the opposite. These results indicate that soil moisture is the key driver of lateral variation in ECa. The EMI results also showed that soil ECa varied laterally and vertically between both 0.5 m and 1.0 m sensor separations across each site, which is expected. Soil aggregate properties such as proportions of sand, silt, and clay are known to influence the bulk electrical conductivity of the soil (e.g. Domsch and Giebel, 2004; Emmanuel et al. 2023). Soil moisture (SM), soil organic matter (OM), cation exchange capacity (CEC) and salinity are all recognized as key factors that govern soil electrical conductivity. For example, previous studies have found that the ECa correlates strongly with soil moisture (SM)

and organic matter (OM) (e.g. Molin and Faulin, 2013; Shanaham et al. 2015). A recent study by Emmanuel et al. (2023) reported a strong correlation between ECa and silt proportion (r^2 = 0.761), and SM (r^2 = 0.702) for restored wetland soils located in Northwest Ohio. They also found that SM correlated with OM, which further suggests that both parameters are somewhat interdependent and thus challenging to decouple. Although some studies observed a slightly stronger influence of OM on soil ECa (e.g., Shanahan et al. 2013; Emmanuel et al. 2023), Domsch and Giebel (2004) argued that SM has a stronger influence on soil ECa, which is probably the case in some wetlands considering that Emmanuel et al. (2023) found their strongest correlation with silt content, which correlated better with SM (r^2 = 0.660) than with OM (0.632).

At our sites, it is possible that an increase in SM due to groundwater level rise could have led to changes in soil water chemistry (e.g., dilution), which would have resulted in the observed temporal variation of the ECa at the CRC transition and wetland zones (See Figure S3). SM varies spatially both laterally across a site and vertically through the soil profile, this is well described by Corwin and Lesch (2005). At these sites, SM was mostly higher at the top 10 cm than at 30 cm depths across the sites except for the periods between June-December when SM was higher at 30 cm (Figure 4c). This implies that the variation of ECa values between 0.5 m and 1.0 m sensor separation is due to variation in SM. EMI could therefore serve as a non-invasive tool for monitoring soil water dynamics to understand ground water-soil water exchanges and their control on biogeochemical processes at land-lake interfaces.

5.2. Geophysics can help reconstruct subsurface stratigraphy

To test the suitability of geophysical methods for characterizing subsurface stratigraphy of land-lake interfaces, we investigated the sites using ERT, GPR and lithologic logs from piezometers.

The ERT results from the three sites (Figure 6) showed relatively lower resistivity values at CRC and PTR in the range of 5.1-74 Ωm than at the OWC site (10.2-148 Ωm). Though the existing wells at the OWC wetland were not deep enough to ground truth the high resistivity values observed in the wetland zone, existing borehole data close to the upland area revealed the presence of dry till at the depth of 50 ft (15m) that could explain the observed higher resistivity. The correlation of the ERT data with lithological logs was very useful in understanding what drives the vertical variation in electrical resistivity across the sites. For example, the high resistivities observed close to the surface in the upland zones of PTR (Figure 10) and OWC (Figure 11) sites were linked to dry silty clay. The results also indicate that similar soil types could show different resistive responses at different sites depending on how their electrical property compares to that of the surrounding material. For example, a layer of till showed very low resistivity values at the CRC upland, while at the PTR site the same till layer appeared as a relatively more resistive layer. This is because, at the CRC upland, the till is surrounded by more resistive silty clay layers, while at the PTR site, the till is overlaid by wet clay layers, which is much less resistive than the till layer.

The GPR method also revealed structural heterogeneity at the study sites; it clearly identified the boundaries between silty loam and clay layers at CRC and OWC and between dry silty clay and clay at the PTR sites. However, the GPR sensitivity at these sites is limited to the top 1.5 m compared to ERT, which provided high-resolution depth sensitivity up to 19.7 m using a 1 m electrode spacing. The poor resolution observed with GPR above 1.5 m depth could be linked to signal attenuation due to high clay content. SM is known to cause signal attenuation in GPR data (e.g. Huisman et al. 2003; Klotzsche et al. 2018; Agbona et al. 2021). This signal attenuation due to water saturation is expected to be more pronounced in wetlands with high water residence time

555 and could also lead to temporal variations in GPR measurement due to seasonal variation in SM
556 in such wetlands.

557 The surficial geology map of the study area shown in Figure 1 indicates that the geology of the
558 area is characterized by lakebed soils (fine textured lacustrine deposits), underlain by glacial till
559 soils. This agrees with the ERT results of this study, which revealed that the stratigraphy is made
560 up of silty clay and clay layers which are lake bed soils (fine textured lacustrine deposits) and two
561 different types of till layers, differing in their composition (Figure 8), which the surficial geology
562 map revealed to be clayey Wisconsin till and loamy Wisconsin till. These tills are rich in clay,
563 which are expected to slow down infiltration and, thus, increase water residence time, which
564 could help to sustain diverse biogeochemical exchanges at these land-lake interfaces. The
565 electrical response of these TAI soils depends on whether they are dry or saturated, this explains
566 why silty clay layers are very resistive in upland areas where they are very dry (see Figure 10),
567 and also why glacial till showed lower resistivity at the CRC site (Figure 9a-b) and high
568 resistivity at PTR site (Figure 10). These results indicate that geophysical methods are useful to
569 reconstruct subsurface stratigraphy of land-lake interfaces.

570

571 **5.3. Geophysics can help improve soil mapping and sampling**

572 One of our hypotheses is that geophysical methods can be used to improve soil mapping and help
573 guide detailed soil sampling. To test this, we studied the site using EMI and then compared the
574 result with USDA soil maps. The close match between the USDA soil maps and the soil ECa
575 maps observed at CRC upland and OWC sites, indicates that the EMI is useful for soil mapping
576 and can be relied upon at sampling restricted sites. Additionally, it is important to note that the
577 ECa maps revealed additional soil units that were not identified from the USDA soil maps. The

soil units mapped by the USDA consist of about 5-15 % sub-units (see Table S1) which were not shown in the soil maps, while the ECa maps provided a more precise detail of the lateral extension of each of these soil units than the soil map, and also identified additional sub-units that were missing in the soil map (Figure 3). Furthermore, the ECa maps reveal that all the hydric soils across the sites (To, Tp and HoA) have high ECa values as shown in Figure 3 and Table D1 (see Table S1), this implies that the EMI could help soil scientists and ecologist to non-invasively map the lateral extent of hydric soils. These results also emphasized the additional value of combining different geophysical methods as a more useful approach to overcome technical limitations associated with single methods by leveraging the strength of each method to bridge the gap in interpretation where other methods are lacking as demonstrated in Figure 12.

6. Conclusions

This work demonstrates the advantage of combining different non-invasive geophysical methods to characterize land-lake interfaces which is a complex and dynamic ecosystem, as no single geophysical method is capable of capturing all the complexities of soil state and processes particularly in a dynamic TAI ecosystem. The close match between ECa maps and USDA soil maps, as well as the additional details provided by the ECa maps, implies that EMI is a useful tool for optimizing soil mapping and could also be used to extrapolate soil properties, particularly at sampling-restricted sites where only non-invasive measurements are feasible.

Unlike the aggregate and the pore approaches of investigating soil architecture which focuses on studying limited core samples, the geophysical methods show a more detailed characterization of soil spatial heterogeneity, with good lateral and vertical resolution. The EMI provided better lateral heterogeneity at high resolution, while ERT and GPR provided high-resolution vertical

variation in the soil profile. The stratigraphy of these land-lake interfaces and their soil moisture dynamics were found to be the key drivers of the observed heterogeneities. Future studies should consider a detailed investigation of temporal variability of the geophysical signals coupled with monitoring temporal changes in SM and soil water quality to better understand the mechanism behind the temporal variation of the ECa observed here, and quantify the influence of fluctuating SM and groundwater levels on the geophysical measurements.

Data Availability Statement

The data associated with this study (Ehosioke et al. 2023) are available in the ESS-DIVE data repository: https://data.ess-dive.lbl.gov/datasets/ess-dive-5fe23e299966ce8-20231007T202450197

Acknowledgements

This research is based on work supported by COMPASS-FME, a multi-institutional project supported by the U.S. Department of Energy, Office of Science, Biological and Environmental Research as part of the Environmental System Science Program. The Pacific Northwest National Laboratory is operated for DOE by Battelle Memorial Institute under contract DE-AC05-76RL01830.

References

Agbona, A., Teare, B., Ruiz-Guzman, H., Dobreva, I. D., Everett, M. E., Adams, T., … Hays, D. B. (2021). Prediction of root biomass in cassava based on ground penetrating radar phenomics. Remote Sensing, 13(23), 1–18. https://doi.org/10.3390/rs13234908

AGIUSA. (2005). Instruction Manual. Austin, TX, USA.

Ameli, A. A., & Creed, I. F. (2017). Quantifying hydrologic connectivity of wetlands to surface water systems. Hydrology and Earth System Sciences, 21(3), 1791–1808. https://doi.org/10.5194/HESS-21-1791-2017

Annan A.P. (2009). Electromagnetic principles of ground penetrating radar. In: Jol HM (ed) Ground penetrating radar theory and applications. Elsevier, Amsterdam, pp 4–38

Baker, G.S., Jordan, T.E., and Talley, J. (2007). An introduction to ground penetrating radar (GPR), *in* Baker, G.S., and Jol, H.M., eds., Stratigraphic Analyses Using GPR: Geological Society of America Special Paper 432, p. 1–18, doi: 10.1130/2007.2432(01).

Baveye, P. C., Otten, W., Kravchenko, A., Balseiro-Romero, M., Beckers, É., Chalhoub, M., … Vogel, H. J. (2018). Emergent Properties of Microbial Activity in Heterogeneous Soil Microenvironments: Different Research Approaches Are Slowly Converging, Yet Major Challenges Remain. Frontiers in Microbiology, 9(AUG). https://doi.org/10.3389/FMICB.2018.01929

Besson, A., Cousin, I., Samouëlian, A., Boizard, H., & Richard, G. (2004). Structural heterogeneity of the soil tilled layer as characterized by 2D electrical resistivity surveying. In Soil and Tillage Research (Vol. 79, pp. 239–249). Elsevier B.V. https://doi.org/10.1016/j.still.2004.07.012

Besson, A., Séger, M., Giot, G., & Cousin, I. (2013). Identifying the characteristic scales of soil structural recovery after compaction from three in-field methods of monitoring. Geoderma, 204–205, 130–139. https://doi.org/10.1016/J.GEODERMA.2013.04.010

Bréchet, L., Oatham, M., Wuddivira, M., & Robinson, D. A. (2012). Determining Spatial Variation in Soil Properties in Teak and Native Tropical Forest Plots Using Electromagnetic Induction. Vadose Zone Journal, 11(4), vzj2011.0102. https://doi.org/10.2136/VZJ2011.0102

Corwin, D. L., & Lesch, S. M. (2003). Application of Soil Electrical Conductivity to Precision Agriculture. Agronomy Journal, 95(3), 455. https://doi.org/10.2134/agronj2003.0455

Corwin, D. L., & Lesch, S. M. (2005). Characterizing soil spatial variability with apparent soil electrical conductivity: I. Survey protocols. Computers and Electronics in Agriculture, 46(1–3), 103–133. https://doi.org/10.1016/J.COMPAG.2004.11.002

Dexter, A. R. (1988). Advances in characterization of soil structure. Soil and Tillage Research, 11(3–4), 199–238. https://doi.org/10.1016/0167-1987(88)90002-5

Domsch, H., & Giebel, A. (2004). Estimation of soil textural features from soil electrical conductivity recorded using the EM38. Precision Agriculture, 5(4), 389–409. https://doi.org/10.1023/B:PRAG.0000040807.18932.80/METRICS

Doolittle, J. A., & Brevik, E. C. (2014). The use of electromagnetic induction techniques in soils studies. Geoderma, 223–225(1), 33–45. https://doi.org/10.1016/J.GEODERMA.2014.01.027

Doro, K. O., Leven, C., Cirpka, O. A. (2013): Delineating subsurface heterogeneity at a River Loop using geophysical and hydrogeological methods. Environ. Earth Sci., 69 (2) 335 – 348 doi:10.1007/s12665-013-2316-0

Emmanuel, E. D., Christian, Lenhart, F., Weintraub, M. N., & Doro, K. O. (2023). Estimating Soil Properties Distribution at a Restored Wetland Using Electromagnetic Imaging and Limited Soil Core Samples. Wetlands 2023 43:5, 43(5), 1–19. https://doi.org/10.1007/S13157-023-01686-3

Franke, R. (1982), Scattered Data Interpolation: Test of Some Methods,Mathematics of Computations, v. 33, n. 157, p. 181-200.

Gebbers, R., Lück, E., Dabas, M., & Domsch, H. (2009). Comparison of instruments for geoelectrical soil mapping at the field scale. Near Surface Geophysics, 7(3), 179–190. https://doi.org/10.3997/1873-0604.2009011

Geonics L (2009) EM38–MK2 ground conductivity meter operating manual, Canada Ontario

Grote, K., Hubbard, S., & Rubin, Y. (2003). Field-scale estimation of volumetric water content using ground-penetrating radar ground wave techniques. Water Resources Research, 39(11). https://doi.org/10.1029/2003WR002045

Halder, S. K. (2018). Mineral Exploration, principles and applications (Second Edition), p. 103-122

Hansen, M. C. (1989). History of Lake Erie. Ohio Geology Newsletter.

Huisman, J. A., Hubbard, S. S., Redman, J. D., & Annan, A. P. (2003). Measuring Soil Water Content with Ground Penetrating Radar: A Review. Vadose Zone Journal, 2, 476–491.

Hurt, G. W., & Vasilas, L. M. (2006). Field indicators of hydric soils in the United States.

Kemna, A., Binley, A., Cassiani, G., Niederleithinger, E., Revil, A., Slater, L., … Zimmermann, E. (2012). An overview of the spectral induced polarization method for near-surface applications. In Near Surface Geophysics (Vol. 10, pp. 453–468). EAGE Publishing BV. https://doi.org/10.3997/1873-0604.2012027

Kessouri, P., Furman, A., Huisman, J. A., Martin, T., Mellage, A., Ntarlagiannis, D., … Placencia-Gomez, E. (2019). Induced polarization applied to biogeophysics: recent advances and future prospects. Near Surface Geophysics, 17, 595–621. https://doi.org/10.1002/nsg.12072

Kizhlo, M., & Kanbergs, A. (2009). The Causes of the Parameters Changes of Soil Resistivity. In Scientific proceedings of Riga Tachnical University (pp. 43–46). https://doi.org/10.2478/v10144-009-0009-z

Klotzsche, A., Jonard, F., Looms, M. C., van der Kruk, J., & Huisman, J. A. (2018). Measuring Soil Water Content with Ground Penetrating Radar: A Decade of Progress. Vadose Zone Journal, 17(1), 0. https://doi.org/10.2136/vzj2018.03.0052

Kravchenko, A., Otten, W., Garnier, P., Pot, V., & Baveye, P. C. (2019). Soil aggregates as biogeochemical reactors: Not a way forward in the research on soil–atmosphere exchange of greenhouse gases. Global Change Biology, 25(7), 2205–2208. https://doi.org/10.1111/GCB.14640

Krüger, J., Franko, U., Fank, J., Stelzl, E., Dietrich, P., Pohle, M., & Werban, U. (2013). Linking Geophysics and Soil Function Modeling-An Application Study for Biomass Production. Vadose Zone Journal, 12(4), vzj2013.01.0015. https://doi.org/10.2136/VZJ2013.01.0015

Loke, M.H. (2000) Electrical Imaging Surveys for Environmental and Engineering Studies. A Practical Guide to 2-D and 3-D Surveys, 61.

703 Maestre, F.T., Cortina, J. (2002). Spatial patterns of surface soil properties and vegetation in a
704 Mediterranean semi-arid steppe. *Plant Soil* 241, 279–291.

705 McBratney, A., Minasny, B., 2007. On measuring pedodiversity. Geoderma 141, 149e154

706 Mertens, F. M., Pätzold, S., & Welp, G. (2008). Spatial heterogeneity of soil properties and its
707 mapping with apparent electrical conductivity. Journal of Plant Nutrition and Soil Science,
708 171(2), 146–154. https://doi.org/10.1002/JPLN.200625130

709 Michot, D., Benderitter, Y., Dorigny, A., Nicoullaud, B., King, D., & Tabbagh, A. (2003). Spatial
710 and temporal monitoring of soil water content with an irrigated corn crop cover using
711 surface electrical resistivity tomography. Water Resources Research, 39(5).
712 https://doi.org/10.1029/2002WR001581

713 Molin, J. P., & Faulin, G. D. C. (2013). Spatial and temporal variability of soil electrical
714 conductivity related to soil moisture. Scientia Agricola, 70(1), 01–05.
715 https://doi.org/10.1590/S0103-90162013000100001

716 Myers, D.N., Thomas, M.A., Frey, J.W., Rheaume, S.J., & Button, D.T. (2000). Water quality in
717 the Lake Erie-Lake Saint Clair Drainages Michigan, Ohio, Indiana, New York, and
718 Pennsylvania, 1996-98: U.S Geological Survey Circular 1203, 35p.
719 https://pubs.water.usgs.gov/circ1203/

720 ODNR (2018). Ohio Coastal Atlas, Third Edition. https://www.coastal.ohiodnr.gov/atlas

721 Osborne, T. Z & Ron D. DeLaune. 2013. Soil and Sediment Sampling of Inundated
722 Environments. Chapter 2, page 21-40. *In:* R. D. DeLaune, K. R. Reddy, C. J. Richardson,
723 and P. J.Megonigal, eds. Methods in Biogeochemistry of Wetlands, Soil Science Society of
724 America. Madison, WI. 1024 pp.

725 Paton, D., & PENSERV Corp, Pa. (2012). An evaluation of the USDA ESAP program for
726 converting EM data to electrical conductivity at Goodale Research Farm using a GEM2 and
727 an EM38. Retrieved from https://harvest.usask.ca/handle/10388/9097

728 Rabot, E., Wiesmeier, M., Schlüter, S., & Vogel, H. J. (2018). Soil structure as an indicator of
729 soil functions: A review. Geoderma, 314, 122–137.
730 https://doi.org/10.1016/J.GEODERMA.2017.11.009

731 Romero-Ruiz, A., Linde, N., Keller, T., & Or, D. (2018). A Review of Geophysical Methods for
732 Soil Structure Characterization. Reviews of Geophysics, 56(4), 672–697.
733 https://doi.org/10.1029/2018RG000611

734 Romero-Ruiz, A., Linde, N., Keller, T., & Or, D. (2019). The Geophysical Signatures of Soil
735 Structure. Eos, 100. https://doi.org/10.1029/2019EO112545

736 Shanahan, P. W., Binley, A., Whalley, W. R., & Watts, C. W. (2015). The Use of
737 Electromagnetic Induction to Monitor Changes in Soil Moisture Profiles beneath Different
738 Wheat Genotypes. Soil Science Society of America Journal, 79(2), 459–466.
739 https://doi.org/10.2136/SSSAJ2014.09.0360

740 SSURGO (2012). Gridded Soil Survey Geographic Database (SSURGO) for Ohio. Available
741 online at the Available online at http://datagateway.nrcs.usda.gov/ October 15, 2012.

Sposito, G. (2023). *soil*. *Encyclopedia Britannica*. https://www.britannica.com/science/soil

Stewart, B. A. (Ed.). (1990). Advances in Soil Science, 14. https://doi.org/10.1007/978-1-4612-3356-5

Subburayalu SK, Slater BK (2013). Soil series mapping by knowledge discovery from Ohio county soil map. SSSAJ 77:1254-1268. Available online at http://datagateway.nrcs.usda.gov/ October 15, 2012.

Totsche, K. U., Rennert, T., Gerzabek, M. H., Kögel-Knabner, I., Smalla, K., Spiteller, M., & Vogel, H. J. (2010). Biogeochemical interfaces in soil: The interdisciplinary challenge for soil science. Journal of Plant Nutrition and Soil Science, 173(1), 88–99. https://doi.org/10.1002/JPLN.200900105

USDA (2019). Soil Survey Staff, Natural Resources Conservation Service, United States Department of Agriculture. Web Soil Survey. Available online at the following link: http://websoilsurvey.sc.egov.usda.gov/.

Vogel, H. J., Balseiro-Romero, M., Kravchenko, A., Otten, W., Pot, V., Schlüter, S., … Baveye, P. C. (2022). A holistic perspective on soil architecture is needed as a key to soil functions. European Journal of Soil Science, 73(1), e13152. https://doi.org/10.1111/EJSS.13152

Ward, N. D., Patrick Megonigal, J., Bond-Lamberty, B., Bailey, V. L., Butman, D., Canuel, E. A., … Windham-Myers, L. (2020). Representing the function and sensitivity of coastal interfaces in Earth system models. Nature Communicationsature Communications, 11(2458). https://doi.org/10.1038/s41467-020-16236-2

Young, I. M., Crawford, J. W., & Rappoldt, C. (2001). New methods and models for characterising structural heterogeneity of soil. Soil and Tillage Research, 61(1–2), 33–45. https://doi.org/10.1016/S0167-1987(01)00188-X

773